TiN ions implantation on SS316L targets by a 4kJ plasma focus facility

Malihe Omrani, Morteza Habibi, Reza Amrollahi

Amirkabir University of Technology, Tehran, Iran

Mortezahabibi@aut.ac.ir

The present work reports the results of TiN-ions implantation on the SS316L samples by a 4 kJ plasma focus device (PF). The thickness of coated layer on the surface of treated samples obtained by RBS analysis is about 15-20 μm. The XRD results reveal the formation of nanocrystalline titanium nitride coating on the surface of substrate. The results of SEM indicate changes in surface morphology before and after potentiostatic test. The ICR results showed that the conductivity of samples increased after coating because of high electrical conductivity of TiN layer. The ICR increased after the potetiostate test because of change in passive layer composition. The electrochemical results show that the corrosion resistances have been improved signficantly when TiN films are deposited on the SS316L substrate. The corrosion potential (E_{corr}) of SS316L implanted with Ti-N ions increases compared with that of the bare SSI316L and corrosion currents decrease in TiN implanted samples.

1. Introduction

Plasma focus (PF) devices can generate short lived (10–100 ns) but high temperature (0.1–2.0 keV) and high density (10^{18}– 10^{20} cm^{-3}) plasma [1,2]. As it depicted in fig.1 in this configuration the electrical discharge starts along the insulator sleeve. After the breakdown an axially symmetric current sheath is driven outward and accelerates towards the end of the central electrode. Then the current sheath moves rapidly towards the axis and collapse like the conventional Z-pinch. Disruption of dense plasma column due to the growth of sausage instabilities is suggested to be responsible for energetic emission of fast neutrons, electrons, ions, hard X-ray and soft X-ray. These devices with energy ranges from a few kJ to MJ are able to generate energetic ions with energy more than few hundreds of keV to

tens of MeV [1]. In recent years, the ion beam generated by PF devices has been used for material processing [3], deposition of nanoparticles [4], thin film deposition, ion implantation [5] and thermal surface treatment [6]. Measurements of the ion energy distribution in a 4.75 kJ PF operating with nitrogen, were performed with a Thomson analyzer, identified as the main ion species N^{+1}, N^{+2} and N^{+3} with a characteristic energy in the range 0.17-4.0 MeV, and total (time integrated) average ion flux 8×10^{12} ions/stereorad [7]. The effect of argon ion irradiation on vacuum-evaporated as-grown Sb2Te3 films in a 3.3 kJ PF device was studied by Rawat etal [8]. They found that ion energy greater than 1 MeV promoted the formation of nonstoichiometric SbxTe12x phase and the oxidation of Sb. Also ion energy less than 1 MeV promoted the formation of single stoichiomeric Sb2Te3 phase and a homogeneous distribution of grain size with preferred orientation. Other groups have reported synthesis of titanium nitride coating on a titanium substrate[9], deposit of titanium nitride thinfilms on Si(100) substrates[10], modification of AISI 316L stainless steel by irradiation with nitrogen ion beams[11] and deposition of nanoparticles and nanostructured cobalt [12]. Malhotra et al reported the formation of zinc oxide nanoparticles using a 4kJ PF device [13].

Ion implantation is a powerful method for modifying the surface of materials. The use of plasma and ion-beam-modified surfaces and surface coatings is continually expanding in engineering disciplines [14, 15]. The purpose of these modifications and treatments is to impart favourable properties, such as wear resistance, corrosion resistance and lubricity, to the surfaces, while at the same time retaining the strength or toughness of the bulk materials. The bombardment of energetic ion beams can modify the structural and chemical properties of surfaces or applied coatings[16]. Applied as a thin coating, TiN is used to harden and protect cutting and sliding surfaces, for decorative purposes (due to its gold appearance), and as a non-toxic exterior for implants. The motor racing industry has been a major user of nitrided titanium components, with successful applications on valves and valve gear, connecting rods, bearings, hubs and other sliding and wearing surfaces [17,18], high corrosion resistance and good oxidization resistance[19]. The combination of high hardness, low friction coefficient and chemical inertness makes metal nitrides[20], widely accepted candidates for forming and cutting tools.

The idea here is to use titanium anode tip of a 4kJ PF device operating with nitrogen gas and to investigate the effect of energetic ion beam irradiation on SS316L samples. Structural properties of TiN coating were analyzed using X-ray diffractometer (XRD). The micro-structure and morphology of the coating were examined by scanning electron microscopy (SEM). Thickness of the elements found on the surface of treated samples were investigated by RBS technique.

2. Mechanism of the surface modification by PF device

The simplicity in operation and high fluences of emitted ions with wide energy range are making the PF device as a promising system for material processing. The ion beam energy of PF device is dumped onto a near surface layer of the material for the duration of a few tens of nanosecond. Consequently, the surface is heated up to several thousand degrees centigrade in a short time and is immediately followed by fast melting and re-solidification. The high cooling rates can result in the production of new phases in the near surface layer. Therefore, ion beams of PF device have drawn considerable attention in surface modification in recent years [21]. In the case of PF device with nitrogen and titanium fitted anode, the emitted electrons and nitrogen ions could sputter the anode material and form corona plasma above the anode surface. The formed plasma includes titanium atoms and high energy titanium ions in addition to the fast electrons[22]. Primarily, two processes occur on the SS316L surface during collision of the accelerated ions with the samples. (1) nitrogen ions accelerate towards the SS316L substrate and deliver energy instantly, causing high thermal gradients. Consequently, high heating and cooling rates are developed into surface layer of SS316L. In addition, the collision results in etching and cleans the substrate surface in prior to the deposition process. (2) Electrons accelerate towards the titanium anode, and ablate the material from anode. The ablated material can interact with reactive nitrogen ions of same shot to form titanium nitride and deposit at SS316L substrate[23,24]. Furthermore, some of the titanium plasma still does not react with generated nitrogen ions and atoms in each shot. Thus the deposited film contains some titanium atoms. Part of these titanium atoms, deposited on the substrate, react with the accelerated nitrogen ions in the next shots through the ion implantation process. Thus, a rich content of titanium nitride is eventually deposited on the film[23].

3. Experimental procedure

The experiments were carried out with a 4kJ Mather type PF device powered by a single capacitor (40μF, 15 kV, 115nH) shown in Fig.1 [9]. The inner electrode is a hollow copper cylinder which its diameter and length is 20 mm and 148 mm, respectively. The outer electrode is composed of six copper rods which forms the shape of a squirrel cage with an inner diameter of 44 mm. For deposition of titanium nitride films, titanium fitted anode was used instead of copper anode. Besides, anode and cathode are separated by Pyrex tube of 48 mm length. The discharge chamber is evacuated down to 10^{-3} mbar and filled with high purity nitrogen gas. When the capacitor is connected, break down occurs along the insulator and the current sheath is driven away toward the titanium fitted anode tip. Finally, the sheath clashes on the axis in the form of a dense plasma cylinder (pinch). The lifetime of the pinch is about 300 ns. The formation of the dense plasma is followed by the onset of sausage instability, enhancing the induced electric field locally. This enhanced electric field, coupled with the magnetic field, accelerates the ions towards the top of the chamber and electrons towards the positively charged anode. As it plotted in Fig. 2, the signals of the Rogowski coil were recorded in every shot to ensure the best performance of the device.

Optimum pressure with Nitrogen as the filling gas at the applied voltage of 12.5 kV determined 3 mbar. The focus shots are fired at a frequency of one shot per minute, at time long enough to ensure thermal relaxation of specimen after being heated by the preceding ion beam.

The substrates were mounted axially above anode at a distance of 10 cm using substrate holder. Energy and the maximum density of ions at the distance of 10 cm from anode tip are 64keV and 5.9×10^{13} cm^{-3} respectively, with single ion pulse of about 140 ns. So the energy flux delivered to the targets is estimated to be 2.69×10^{13} $KeV\,cm^{-3}nsec^{-1}$. The austenitic stainless steel 316L was used as the substrate material. chemical composition (wt.%) of SS316L is shown in table 1. Samples of SS316L with 2mm thick were cut into 2cm × 2cm specimens for ion implantation and subsequent tests. Before ion implantation, the samples were polished with No. 200, 400, 600, 800, 1200 SiC waterproof abrasive papers and No. 5 diamond paste polisher. The thin films were deposited with different

number of focus shots at 10 cm from the anode tip. Four different films were deposited using 10, 20, 30 focus shots. After every 4 shots, the discharge chamber was evacuated and the fresh nitrogen gas was filled in order to minimize the impurities. Structural properties of TiN coating were then analyzed using SEM, RBS and XRD techniques.

4. Results and discussion

4.1. SEM results

Fig. 3 shows the microstructures of the unexposed SS316L substrate with manual polishing marks and the samples exposed with 10, 20 and 30 shots by using the field emission SEM. A view of the nitride surface depicts multidimensional granular structures of 100 -200 nm size having distinct boundaries. For 10 focus shots ion irradiation, the average size of grains varies from 100 to 300 nm. The number of grains is lower rather than the 20 and 30 shots samples, and the grains don't have sharp boundaries and significant uniformity, whenever a few voids can be seen on the surface. A network structure can be seen in specimen exposed to 20 numbers of focus shots. The surface of the sample exposed to 20 focus shots, has been uniformly covered by the grains which are 100-300 nm in size. The uniform points with an approximated 0.6 nm size are seen on the all of grains. A few voids are seen, and sharp interfaces were observed between the grains. The number of voids is smaller than that of the 10 shots samples, but the interfaces are sharper between the grains. The average particle size of the agglomerated particles in Fig. 4(d) is about 80 nm to 100 nm, but, they are still made up of much smaller size particle with the typical dimension of about 20-30 nm. The agglomeration process arises upon the increase of the number of deposition shots, which can be attributed to more materials amount being ablated and thermal energy carried by material ions was transferred to the sample which cause the small size particles agglomeration[25]. The sample deposited with 30 focus shots has less uniformity rather than the grains in the 20 shots sample. The same as the other samples, a few voids are seen, but in contrast, a few narrow cracks can be observed in the 30 shots sample.

4.2 XRD analysis

In order to specify the formed phases through coating operation, microscopic structure of coated samples has been investigated by XRD analysis. This analysis has been done in

range of 30-100 degree using CuKα_1 radiation. The XRD patterns of the untreated and treated stainless steel AISI 316L are shown in Fig. 4.

High density of high energy-short pulse time (~140nsec) ion beams produced by PF device causes suddenly melting and cooling of sub layer substance. Finally, because of ionic tension, the main phases of crystals were formed by development of the new phase on the surface of melting sample. Crystalline size of deposited TiN layer in 10 cm axial distance from anode tip can be calculated from Scherrer formulae. The crystalline size depends on ion beam energy, and consequently temperature of the sub layer. The smaller grains usually can be seen far from axial positions in sub layers having lower temperature.

In fig. 4 formation of TiN nanocrystalline phases which are obvious in SEM picture is observed. In addition, the peaks showing formation of FeN and Ni_4N crystals can be seen.

The diffraction peaks corresponding to (2 0 0), (2 2 0) and (3 1 1) of TiN crystalline planes are observed on all samples, 10 shots sample and 20 shots sample, respectively. The golden color of deposited films on SS316L substrate also confirmed the presence of TiN films.

The intensity of the TiN (2 0 0) peak for 10 shots sample at 43.02° [14, 16], is much higher than that of other samples. In this figure, the (1 1 1), (2 2 0), (2 0 0) and (0 2 1) peaks of the 10 shots sample are illustrated. It shows the presence of precipitates including TiN (2 0 0) at 2θ=43.02°, TiN (2 2 0) at 2θ=63.2° [26], TiN (2 2 2) at 2θ=79.75°. The peaks of the 10 shots sample are different rather than the other samples, and intensity of TiN(2 0 0) at 2θ=43.02° decreases with increasing the number of shots.

For the 30 shots sample, TiN (2 0 0) at 2θ=41.79° and Ti_2N at 2θ=87.6°, and Ni_4N at 2θ=49.15° peaks are illustrated. In addition, the wider peaks placed at 41.79°, 49.15° and 72.18° correspond to overlapped phases from TiN and FeN, Fe and FeN, and FeN and Ni_4N, respectively.

In the 20 shots sample, the peak related to TiN (2 0 0) and TiN (3 1 1) is seen at 43.34˚ and 74.21˚ respectively [14, 16], and also, the peak at 43.34˚ can be related to Fe_2N (4 0 0).

For the 20 and 30 shots samples, the peaks related to Ni_4N (2 0 0) is observed at 49.15˚, but in 10 shots sample, this phase has not been formed showing formation of Ni_4N crystalline phases with increasing the number of shots. The TiN nanocrystallite size calculated from Scherrer formulae for (3 1 1), (2 0 0) and (2 2 0) diffraction reflections are given in Table I.

4.3 RBS

For measuring the atomic composition of the coatings, RBS was performed using He^{2+} ion beam with energy of 2.4 MeV and a total dose of approximately 10 μC. The RBS spectra were obtained using a 2.5MeV Van de Graaf accelerator. The experiments were performed using Proton beam with 1.8 MeV and Helium beam with 2.4 MeV energy. The longer duration of PIXE analyses by helium beam leads to a better peak resolution. Therefore they were more accurate than Proton analysis for sample diagnostics. The energy and the particles diffracted from surface of sample can be measured by the surface barrier detector of this device. This information is transferred to a computer program, and the output is a diagram that its peaks reveal compounds existing in the sample. Moreover, this software reports the thickness of the elements and also the type of reactions which have been revealed by this analysis.

Fig. 5 shows the PIXI spectra of the coatings deposited on SS316L substrate in this study. all the existence elements in the samples except nitrogen that was indistinguishable by this method were obvious. On the other hand all the existence elements in different layers of sample were indicated that nitrogen and titanium also indexed.

Thickness of the elements found on the surface of treated samples and thickness of coated layer were calculated from the spectra and shown in Table II. The thickness of the thin films were analyzed using SIMNRA software and approximately were in the range of 15-20μm.

5. Conclusions

It can be concluded that PF device is indeed a novel device for nanoparticle deposition. TiN films have been deposited onto SS316L using a 4kJ PF device. Four different thin films were deposited using 10, 20, 30 focus shots. The emitted electrons and nitrogen ions sputter Ti ions from the anode material, and form charged nucleates of TiN, which are deposited on the substrate. SEM images illustrated some points on the surfaces of specimen and that confirms the formation of nanocrystal compounds such as TiN and FeN on the surface of SS316L substrate. The average particle size of the agglomerated particles is about 80 nm to 300 nm. XRD results confirmed the formation of a nanocrystalline TiN layer with an average crystallite size of about 30 nm. XRD results showed the formation of TiN, Ti_2N, FeN and Ni_4N on the surface of SS316L substrate. Also the results showed formation of Ni_4N

crystalline phases with increasing the number of shots. RBS results showed the magnitude of nitrogen and titanium on the surface of the treated samples.

6. References

[1] J. W. Mather, v.8, p.336, Phys. Fluids, (1965)
[2] N. V. Filippov etal, pt.2, p.557, Nuclear Fusion, (1962)
[3] R.S. Rawat *et al.*, Phys. Rev. B 47, 4858 (1993)
[4] W.P. SINGH and M.P. SRIVASTAVA, J. Plasma Fusion Res. SERIES, Vol. 8 (2009)
[5] J.N. Feugeas *et al.*, Rad. Eff. Def. Solids 128, 267 (1994)
[6] A. Shyam and R. K. Rout , IEEE TRANSACTIONS ON PLASMA SCIENCE, VOL. 25, NO. 5(1997)
[7] H. Kelly *et al.*, IEEE Trans. Plasma Sci. 25, p.455 (1997).
[8] R.S. Rawat *et al.*, Materials Research Bulletin 35 (2000) 477–486
[9] A. Qayyum *et al.*, Nuclear Instruments and Methods in Physics Research B 267 (2009) 1911–1917 -(7)
[10] Tousif Hussain et al., Nuclear Instruments and Methods in Physics Research B 267 (2009) 768–772 -(4)
[11] J. Feugeas et al., Surface & Coatings Technology 204 (2010)
[12] W.P. SINGH and M.P. SRIVASTAVA, J. Plasma Fusion Res. SERIES, Vol. 8 (2009)
[13] Y. Malhotra *et al.*, Journal of Physics: Conference Series 208 (2010) 012106
[14] M. Afrashteh, *et al.*, Journal of Fusion Energy, DOI:10.1007/s10894-011-9463-7, (2011)
[15] M. Habibi, R. Amrollahi, Journal of Fusion Energy, 29:481–485 (2010)
[16] M. Hassan, *et al.*,Vacuum, 81 (2006) 291-298
[17] S.B. Hu *et al.*, Surface and Coatings Technology, 141 2001 174181-(21)
[18] Fengqun Lang, Zhiming Yu, Surface and Coatings Technology, 145 (2001) 8087 –(22)
[19] Chun-sheng Ren *et al.*,Vacuum 72 (2004) 41–46 –(23)
[20] Da-Yung Wang, Ming-Chieh Chiu, Surface and Coatings Technology 156 (2002) 201–207-(24)
[21] S.R. Mohanty *et al.*, Nuclear Instruments and Methods in Physics Research B 243 (2006) 113–118
[22] Sh. Al-Hawat, M. Soukieh, M. Abou Kharoub, W. Al-Sadat
[23] G.R. Etaati, et al, Nuclear Instruments and Methods in Physics Research B 269 (2011) 1058–1062
[24] Tousif Hussain , R. Ahmad *, I.A. Khan , Jamil Siddiqui , Nida Khalid, Arshad Saleem Bhatti , Shahzad Naseem, Nuclear Instruments and Methods in Physics Research B 267 (2009) 768–772 -(4)
[25] R. S. Rawat, *et al.*,, Proceedings of the International Workshop On Plasma Computations & Applications (IWPCA2008)
[26] Li Chen, et al, International Journal of Refractory Metals & Hard Materials 26 (2008) 456–460.

Table I. The relationship between the TiN crystallite size (nm) and numbers of focus shots.

No.of shots	TiN crystallian size calculated for different XRD planes (nm)			Mean size (nm)
	(2 0 0)	(2 2 0)	(3 1 1)	
10 shots	37.6	22.28		29.94
20 shots	30.47		35.33	32.9
30 shots	30.46		28.23	29.34

No. of shots	Thickness of elements			thickness of coated layer (μm)
	Ti%	N%	Fe%	
10 shots	53	42	5	15.649
20 shots	20	60	20	21.222
30 shots	20	55	25	20.475

Table II. Thickness of elements and coated layer using RBS

Fig.1. Schematic diagram of PF device

Fig.2. (a) A picture of APF PF device , (b) Inner electrode (Anode), outer electrode (Cathode) and Pyrex

Insulator, (c) Typical discharge current signal with nitrogen at V = 12.5 kV and P = 3 mbar

Fig.3. SEM micrographs of: (a) the substrate surface, (b) 10 shots, (c) 20 shots and (d) 30 shots sample.

Fig. 4. X-ray diffractograms untreated and treated stainless steel AISI 316L.

Fig. 5. PIXI diagrams of the treated AISI 316L samples.

Fig. 6. Typical RBS spectra of the treated AISI 316L sample .

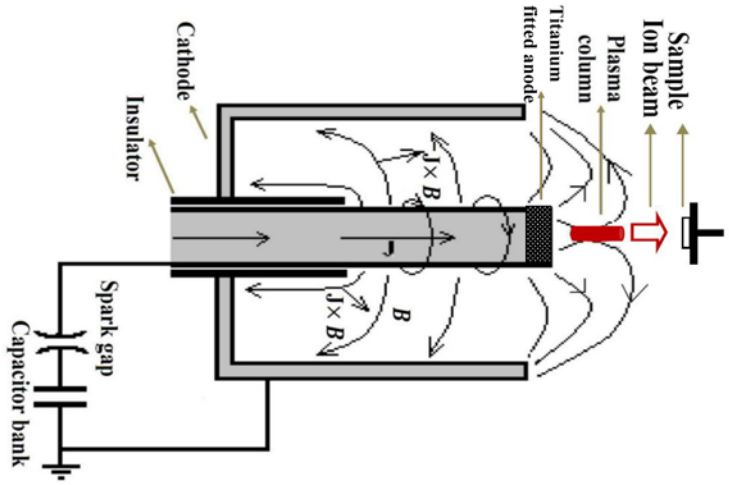

Fig. 1

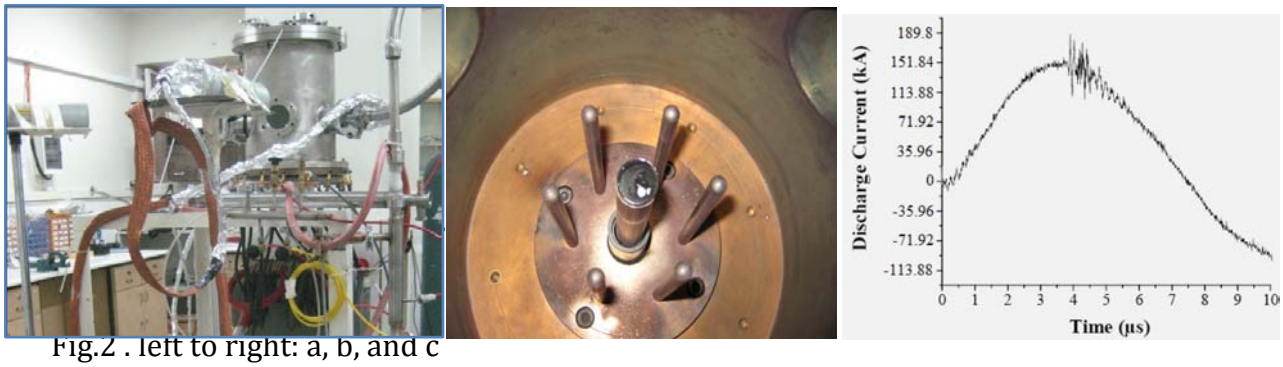

Fig.2 . left to right: a, b, and c

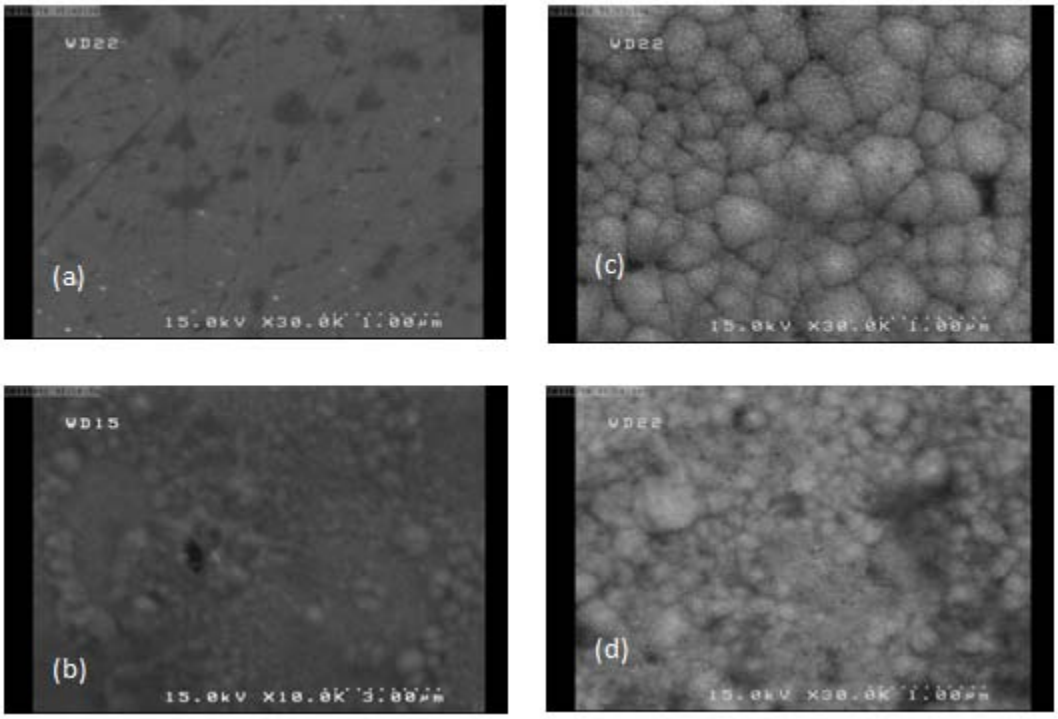

Fig. 3

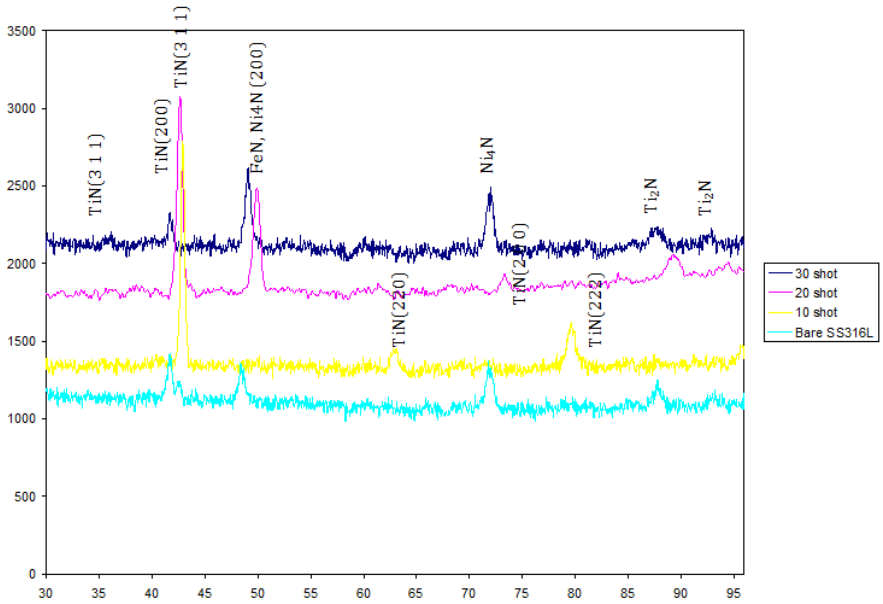
TiN(3 1 1)
TiN(200)
TiN(3 1 1)
FeN, Ni4N (200)
Ni4N
TiN(220)
TiN(220)
TiN(222)
Ti2N
Ti2N
30 shot
20 shot
10 shot
Bare SS316L

Fig. 4

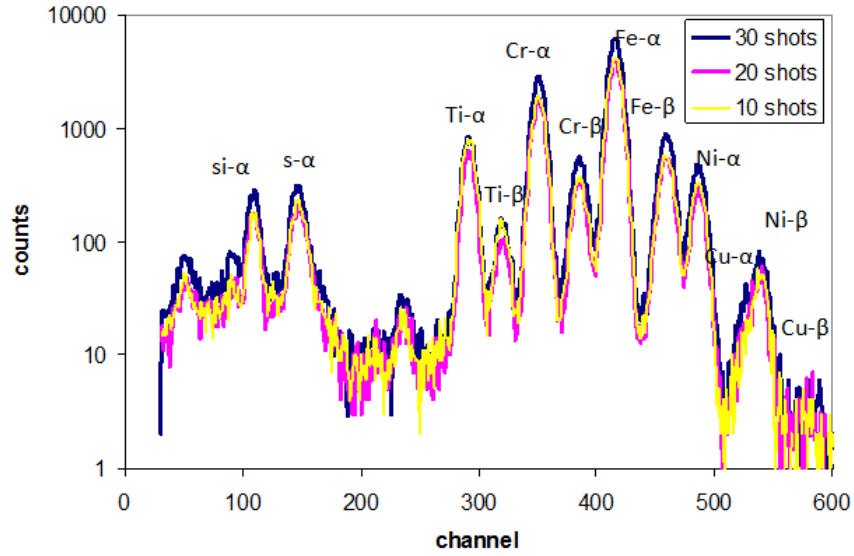
counts
channel
30 shots
20 shots
10 shots
si-α
s-α
Ti-α
Ti-β
Cr-α
Cr-β
Fe-α
Fe-β
Ni-α
Ni-β
Cu-α
Cu-β

Fig. 5

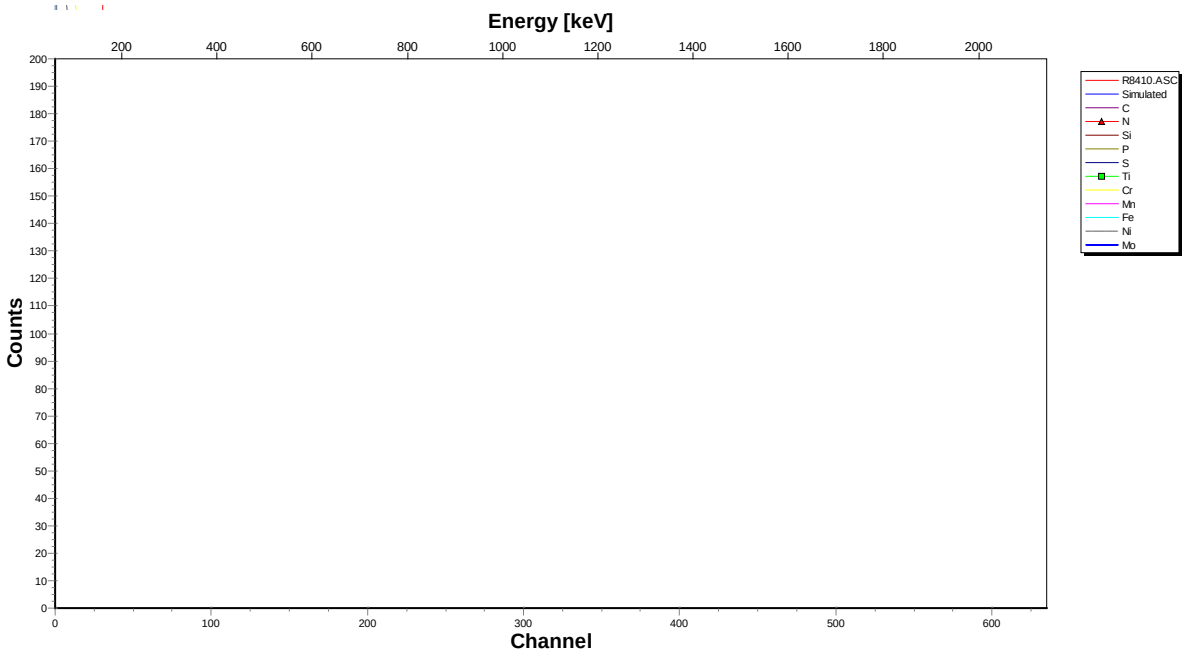
Energy [keV]
200
400
600
800
1000
1200
1400
1600
1800
2000
Counts
0
10
20
30
40
50
60
70
80
90
100
110
120
130
140
150
160
170
180
190
200
Channel
0
100
200
300
400
500
600
R8410.ASC
Simulated
C
N
Si
P
S
Ti
Cr
Mn
Fe
Ni
Mo

Fig. 6